

Coherent Diffraction Imaging of Single 95nm Nanowires

Vincent Favre-Nicolin,^{*} Joël Eymery, Robert Köster, and Pascal Gentile

CEA, INAC, F-38054 Grenoble, France[†]

(Dated: May 19, 2022)

Photonic or electronic confinement effects in nanostructures become significant when one of their dimension is in the 5-300 nm range. Improving their development requires the ability to study their structure - shape, strain field, interdiffusion maps - using novel techniques. We have used coherent diffraction imaging to record the 3-dimensionnal scattered intensity of single silicon nanowires with a lateral size smaller than 100 nm. We show that this intensity can be used to recover the hexagonal shape of the nanowire with a resolution of ≈ 15 nm. The article also discusses limits of the method in terms of radiation damage.

PACS numbers: 61.46.Km, 62.23.Hj, 61.05.cp, 42.30.Rx

Keywords: Nanowires, coherent diffraction, synchrotron radiation, radiation damage

Vertical semiconductor nanowires (NWs) are developed as new, nanoscale building blocks for future electronic and photonic devices. For all applications, the properties depend strongly on the individual crystal structure and the average characteristics of the assembly of NWs. For some applications (resonant sensors, optical microcavities), device operation requires precise and matching characteristics (like diameters, longitudinal insertions or core/shell thicknesses) on many NWs. To characterize the structural properties of these new materials, transmission electron microscopy (TEM) is a standard tool that gives accurate information about individual objects when they are small (diameter < 20 nm).

X-ray diffraction is also a choice method to study nanostructures,¹ particularly when chemical sensitivity (using anomalous scattering²) or strain mapping is required. But there is limited number of X-ray diffraction studies on nanowires³, due to the fact that for many samples it is not possible to perform a quantitative study on an *assembly* of NWs: lack of an epitaxial relationship between the substrate and the vertical NWs, too large angular distribution of the wires, etc.. In this case it is required to conduct diffraction experiments on *single* NWs. To this end, Coherent Diffraction Imaging (CDI) has been developed during the last few years:⁴ in this method, scattering from a single object is recorded

around one Bragg peak, and the recorded 3D data can be inverted to recover the shape of the scattering object. State of the art recent results show that it is now possible to study objects down to a few hundreds of nm in size, and more importantly that CDI allows to probe deformation inside a nanocrystal.⁴ Existing studies have been focalised mostly on model materials with heavy atoms to yield a strong scattering of the X-ray beam (e.g. Pb and Au droplets).

In the case of NWs, optical confinement effects begin to occur around 100-300 nm diameter (depending on the material), and electronic confinement around 5-30 nm.^{5,6} It is therefore of particular importance to study *small* wires, with a diameter of the order of 100 nm. To evaluate the possibility of using CDI for sub-100 nm wires, we conducted an experiment with homogeneous nanowires on the ID01 beamline of the European Synchrotron Research facility.

The silicon NWs (see Fig. 1) were grown by low pressure (20 mBar) chemical vapor deposition at 650°C via the gold-assisted Vapor-Liquid-Solid mechanism on (111) silicon substrate. Au droplets defining the NW size were obtained by dewetting of 2D layers and silane (15 sccm) diluted in hydrogen was used as the reactive gas. The advantage of these Si NWs is that they are known to grow with little or no defects -particularly stacking faults along the [111] direction- which is vital in a CDI experiment since it is required that all atoms diffract in a coherent manner. In the case of faulted NWs the scattered signal would be vastly different.^{7,18}

During the experiment, the epitaxial wires were removed from the substrate and deposited on another silicon substrate, thus producing a random orientation for all the wires - this method decreases the likelihood that two different wires will diffract simultaneously on the detector for a given orientation of the sample, so that the diffraction of a single wire can be recorded. The sample was placed under He atmosphere to prevent oxidizing.

The experiment was carried out using an X-ray photon energy equal to 10 keV, using beryllium compound refractive lenses⁸ to focus the beam to $8.2 \times 13.6 \mu\text{m}^2$ (larger than the NW lengths), with a photon flux equal to

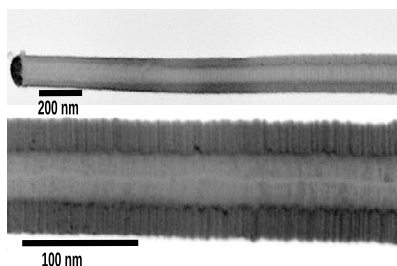


FIG. 1: Scanning electron microscopy images of a silicon nanowire, with an hexagonal-shaped section. The gold droplet used as a catalyst for the synthesis can be seen at the top of the wire (upper view). The bottom view shows the facets and nano-facetting for the same wire.

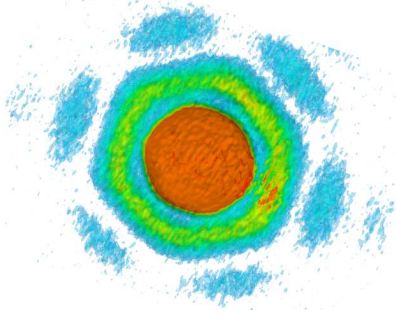


FIG. 2: (color online) 3D coherent diffraction image of a single Si $\langle 111 \rangle$ nanowire, shown as a projection of multiple semi-transparent iso-surface layers, with the intensity increasing logarithmically from blue to green and red. The hexagonal symmetry of the wire is visible in the 3D diffraction image.

4×10^{10} ph/s. The scattered intensity was measured using a Roper Scientific (SX-1300B) direct-illumination CCD, to obtain a maximum resolution and photon-counting efficiency.⁹ This detector presents $20 \mu\text{m}$ pixels and was placed at 743 mm from the sample.

In order to collect the 3D scattered intensity around one Si (111) Bragg peak, the detector was placed at the Bragg angle corresponding to the reflection, and the sample was then translated and/or rotated until one NW diffracted on the detector. Goniometer translations were used to ensure that the NW remains at the intersection of the X-ray beam and of the horizontal rotation axis. The complete scattering was then recorded using a $\pm 0.5^\circ$ oscillation scan with 0.01° steps to yield a 3D pattern, which is then projected to an orthonormal frame of reference in reciprocal space (see Ref.¹⁰ for details on the conversion between detector and reciprocal space coordinates) ; a view of the corrected 3D pattern is shown in Fig. 2.

In the case of a single, non-strained nano-object subjected to an incoming coherent plane wave, the scattered amplitude A is equal to :

$$A(\mathbf{k}) = F(\mathbf{k})FT[\Omega(\mathbf{r})] \quad (1)$$

where $\mathbf{k} = \mathbf{k}_f - \mathbf{k}_i$ is the scattering vector near the $\mathbf{k}_{\text{Bragg}}$ Bragg position, $F(\mathbf{k})$ is the structure factor of a single unit cell, $FT[\Omega(\mathbf{r})]$ is the Fourier transform (FT) of the shape function $\Omega(\mathbf{r})$ of the nano-crystal, *i.e.* a function which is equal to 1 inside the crystal and 0 outside.¹⁹ As the structure factor is slowly varying near an existing Bragg peak, we can further assume that $F(\mathbf{k}) \approx F(\mathbf{k}_{\text{Bragg}})$ and therefore that the scattered amplitude is the 3D FT of the nanocrystal's shape - or equivalently to its electronic density profile.

During a CDI experiment only the square modulus of the amplitude is collected, and all phase information is lost. It is however possible to recover the lost phases using *a priori* information on the object - in our case the inverse FT of the scattered amplitude corresponds to the electronic density of the sample and must be real, *positive, compact and finite-sized*. These criterion have been

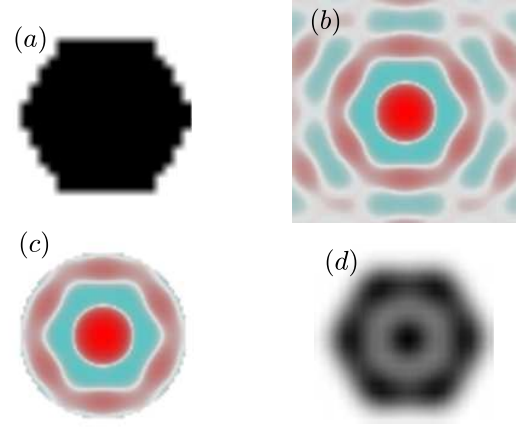


FIG. 3: (color online) Simulation of the truncation effect on the reconstruction of a NW shape. (a) original hexagonal shape of the NW ; (b) FT of the NW shape: as the original shape is centrosymmetric, the FT is real, here depicted with positive regions in red and negative in blue ; (c) truncation of the FT and (d) resulting NW shape calculated by inverse FT, in which dips can be clearly seen due to the truncation.

used in a number of Fourier-recycling algorithms^{11,12,13,14} to retrieve the phase corresponding to each point of the 3D reciprocal space.

In our case the recorded intensity, shown in Fig. 2, exhibits a clear sixfold symmetry which suggests that the original $\langle 111 \rangle$ wire was hexagonally-shaped, as exhibited on most wires by scanning electron microscopy (SEM). Furthermore, the calculation of the FT of an hexagon shape reveals that the phase is either 0 or π (due to the presence of a center of symmetry), as shown in Fig. 3, and presents concentric hexagonal-shaped rings with *alternated* $0/\pi$ phases. In order to reconstruct the shape of the NW 2D cross-section²⁰, we projected the recorded intensity onto the plane perpendicular to the wire and applied an alternated sign ($+1/-1$) to the concentric rings (see Fig. 4a) and then computed the inverse FT to yield the shape of the NW, which can be seen in Fig. 4b.

The obtained shape of the NW exhibits the expected hexagonal symmetry. In order to check that the 'alternating $0/\pi$ phases' was the correct solution to the lost phases, we checked (see Fig. 4c) that the real part of the inverse FT was strictly positive inside the object, and much larger than the imaginary part (ratio $\frac{\text{Real}}{\text{Imag}} > 50$), which validates the phase choice. Note that this outcome was not guaranteed, as the original data was not *strictly* centrosymmetric, and no attempt (*e.g.* by symmetry averaging) was made to modify this.

The size (FWHM distance between opposite faces) of the wire is $\approx 95 \text{ nm}$, with a resolution of about 15 nm for the reconstruction ; the NW appears to be slightly elongated in one direction, which may be due to an asymmetric NW growth, probably due to the original seed combined with kinetic limitations. In the extracted density

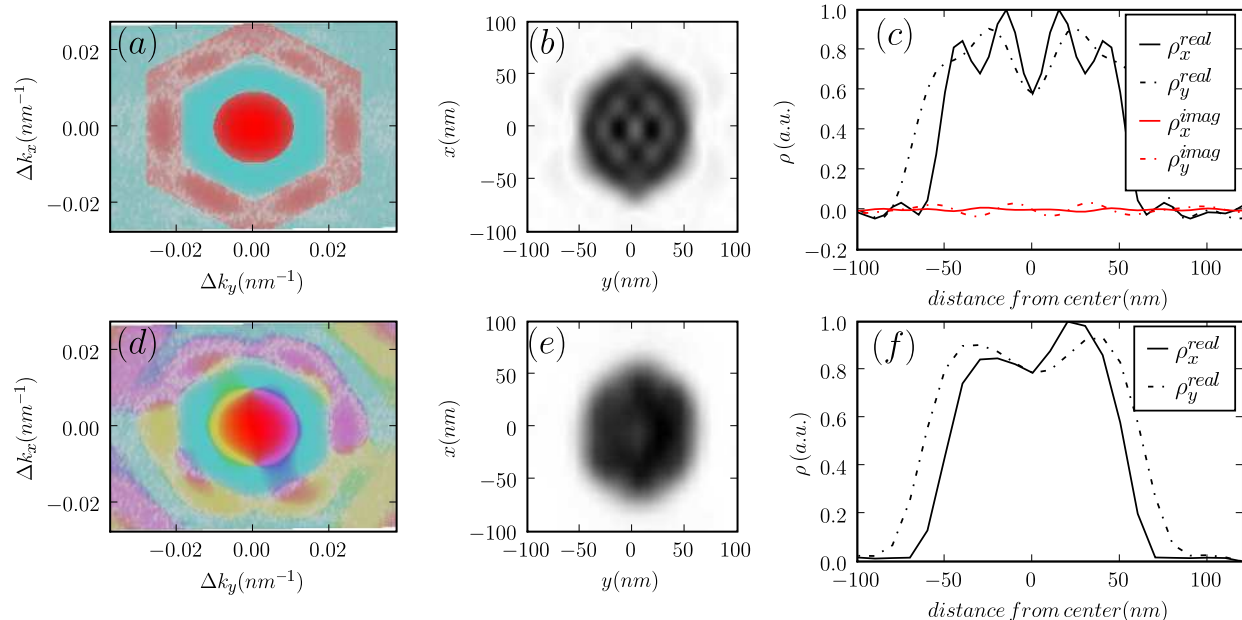


FIG. 4: (color online) The real shape (electronic density) of the NW can be reconstructed from the measured scattered amplitude by recovering the lost phase information, either by *guessing* the phase values (a-b-c) or by using *Fourier recycling algorithms* (d-e-f) (see text for details) (a) projection of the experimental scattered amplitude, with model phases - blue for positive regions and red for negative ones (see text for details). Relative coordinates around the (111) reflection are given in $k = 2 \sin \theta / \lambda$ units. (b) NW density cross-section, obtained by inverse Fourier transform of (a) ; the distance between opposite facets is equal to $\approx 95 \text{ nm}$. (c) density profiles along the horizontal (ρ_x) and vertical (ρ_y) directions, which demonstrate (the real components being positive and the imaginary one negligible) that the choice of alternating (+) and (-) sign for successive rings is correct. The dips of the density inside the NW are due to the limited extent of the intensity scattered by the silicon NW. (d) Experimental amplitude with the phase (colour-coded) recovered using *ab initio* Fourier-recycling algorithms. (e) the best reconstruction obtained and (f) the corresponding cross-sections (positivity is imposed in the algorithm).

map shown in Fig. 4b, we observe a variation amounting up to 20% from the average value. This is very likely due to the limited extent of the recorded intensity: only three interference orders (0,1,2) have been recorded, due to the small size of the NW and the weak scattering power of the silicon atoms, which both limits the real-space resolution and can create ripples inside the reconstructed density ; a simulation of the effect of truncated data is presented in Fig. 3 and has allowed us to reproduce the electronic density dips (Fig. 3d). Another source for the limited resolution on the sides of the NW comes from the zig-zag nature of the NW facets (see Fig. 1), which blurs the average density on the NW borders.

In order to check that the reconstructed structure using alternating phases was the best possible, we also performed an *ab initio* reconstruction using a combination of the error-reduction, hybrid input/output and charge flipping algorithms, using finite support and positivity as constraints, following the process depicted in Ref.¹¹. The best set of phases that we obtained²¹ (see Fig. 4d,e,f) has an R-factor¹¹ equal to 0.7%, features the expected alternating phases, and the reconstructed NW shape also presents a quasi-hexagonal shape, thus confirming the results of the inversion using "guessed phases".

One expected problem when studying single, nano-sized objects using an X-ray beam is radiation dam-

age: this is a well known issue for macromolecular compounds^{15,16}, with a dose limit estimated to 2.10^7 Gy ($1 \text{ Gy} = 1 \text{ J/kg}$). In the case of inorganic compounds there is no acknowledged dose limit, as the compounds do not present the specific weak bonds ($-\text{CO}_2$, $\text{S} - \text{S}$) that are likely to break under irradiation.

We have however observed that the NW can break under the X-ray beam, as is illustrated in Fig. 5. We measured the scattering from a single wire using a $\pm 0.8^\circ$ oscillation scan, with 0.02° angular steps, and a 50 s exposure time per image. This was repeated four times in order to accumulate more statistics, and the evolution of the projection of the 3D recorded scattering is shown in Fig. 5. During this measurement, the flux of the experiment was equal to $\approx 4 \text{ ph/s/\AA}^2$. Given the silicon absorption cross-section $\sigma_{E=10 \text{ keV}} = 1.5 \times 10^{-5} \text{ \AA}^2$, this results in a absorbed power per atom of 0.6 eV/s , or equivalently $2 \times 10^6 \text{ Gy/s}$, *i.e.* a total dose of $8 \times 10^9 \text{ Gy}$ per scan.

During the experiment, the absorbed energy is not accumulated and can be evacuated through fluorescence, thermal radiation or conductivity, but point defects will nevertheless be created in the sample. The presence of already existing defects (such as a stacking fault - a common occurrence in NW¹⁷, point defects or dislocations) can however be considered as a "weak" part of the struc-

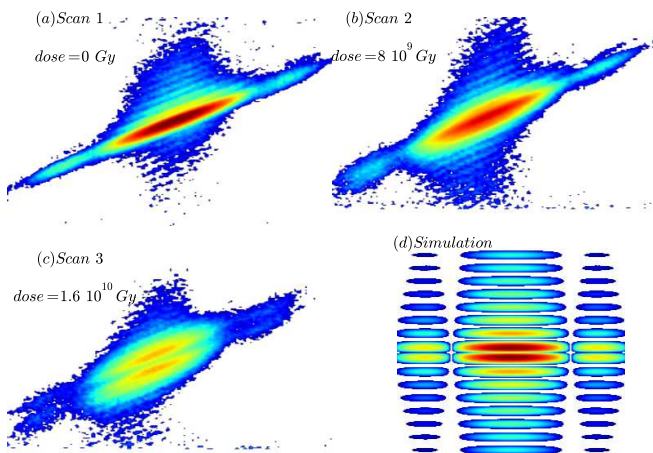


FIG. 5: (color online) Effect of radiation damage: (a,b,c) evolution of the 3D diffraction pattern of a single Si NW around the (111) reflection for successive scans, with a total exposure time of 4000 s per scan (a fourth scan is not presented here). The projection is presented in the direction perpendicular to the NW axis, using a logarithmic colour scheme. The short vertical oscillations are due to the finite length of the wire, and disappear in later scans, due to the breakage of the NW. The fringes which can be seen parallel to the diagonal of the image correspond to the FT of the NW cross-section, as seen in Fig. 2 for another wire. Note that the image presented here is a raw projection of the 3D data, and is not orthonormal in reciprocal space. The split of the main diffraction peak could be due to a break of the NW: (d) simulated scattered amplitude around the (111) reflection of a broken wire, with two parts with an equal length of 800 111 planes and a width of 190 $\bar{1}\bar{1}0$ planes, with a separation between the two parts equal to half the interplanar distance d_{111} . The vertical (resp. horizontal) axis correspond to the 111 (resp. $\bar{1}\bar{1}0$) direction. This separation leads to two maxima at the (111) reflection position.

ture, which could lead to a broken wire as exhibited in Fig. 5.

In conclusion, we have demonstrated that it was possible to use coherent diffraction imaging on single ≈ 100 nm NW to recover their shape with a ≈ 15 nm resolution, even in the case of weak scatterers like silicon. Evidently the interest of this result does not lie in the reconstruction of the shape of homogeneous NW, since scanning and transmission electron microscopy routinely yield the external shape of nano-sized object with a better resolution. However this technique will be particularly useful in the case of **heterogeneous NW**, *i.e.* with longitudinal or radial (core-shell) heterostructures: these type of NW exhibit strain fields and chemical gradients at the interface for which which X-ray diffraction remains the most sensitive technique, and will be the focus of upcoming experiments.

Moreover constant progress is made for X-ray optics in order to improve the coherence and flux on synchrotron beamlines - the focused beam size on the ESRF ID01 beamline was limited by vibrations of the optics which have now been eliminated, yielding a significantly higher flux (10^{10} ph/s in $2.5 \times 0.5 \mu\text{m}^2$), and therefore allowing a better resolution, and the ability to study smaller NWs.

This work has been partially performed under the EU program NODE 015783. The authors would like to thank the ID01 ESRF beamline for their technical help, and acknowledge Prof. Ian Robinson for helpful discussions.

* Also at Université Joseph Fourier, Grenoble France; Electronic address: Vincent.Favre-Nicolin@cea.fr

† URL: <http://inac.cea.fr/sp2m/>

¹ V. H. J. Stangl and G. Bauer, Reviews of Modern Physics **76**, 725783 (2004).

² A. Létoublon, V. Favre-Nicolin, H. Renevier, M. G. Proietti, C. Monat, M. Gendry, O. Martry, and C. Priester, Phys. Rev. Lett. **92**, 186101 (2004).

³ J. Eymery, F. Rieutord, V. Favre-Nicolin, O. Robach, Y.-M. Niquet, L. Frberg, T. Martensson, and L. Samuelson, Nano Letters **7**, 2596 (2007).

⁴ M. Pfeifer, G. Williams, I. Vartanyants, R. Harder, and I. Robinson, Nature **442**, 63 (2006).

⁵ Y. Li, F. Qian, J. Xiang, and C. M. Lieber, Materials Today **9**, 36 (2006).

⁶ P. J. Pauzauskie and P. Yang, Materials Today **9**, 18 (2006).

⁷ V. Chamard, J. Stangl, S. Labat, B. Mandl, R. T. Lechner, and T. H. Metzger, J. Appl. Cryst. **41**, 272 (2008).

⁸ A. Snigirev, V. Kohn, I. Snigireva, A. Souvorov, and B. Lengeler, Applied Optics **37**, 653 (1998).

⁹ F. Livet, Acta Cryst. **A63**, 87 (2007).

¹⁰ V. Favre-Nicolin, S. Bos, J. E. Lorenzo, P. Bordet, W. Shepard, and J.-L. Hodeau, J. Appl. Cryst. **33**, 52 (2000).

¹¹ J. S. Wu and J. C. H. Spence, Acta Cryst. **A61**, 194 (2005).

¹² R. W. Gerchberg and W. O. Saxton, Optik **35**, 237246 (1972).

¹³ J. R. Fienup, Appl. Opt. **21**, 2758 (1982).

¹⁴ S. Marchesini, H. He, H. Chapman, S. Hau-Riege, A. Noy, M. Howells, U. Weierstall, and J. Spence, Phys. Rev. B **68**, 140101 (2003).

¹⁵ S. Marchesini, H. N. Chapman, S. P. Hau-Riege, R. A. London, and A. Szoke, Optics Express **11**, 2344 (2003).

¹⁶ J. W. Murray, E. F. Garman, and R. B. G. Ravelli, J. Appl. Cryst. **37**, 513 (2004).

¹⁷ M. A. Verheijenand, G. Immink, T. de Smet, M. T. Borgström, and E. P. A. M. Bakkers, J. Am. Chem. Soc. **128**, 1353 (2006).

¹⁸ We have also studied the case of GaAs/GaP [111] NWs which are known for their stacking faults along the growth direction. In such a case, the CDI signal recorded is essen-

tially be a function of the faults nature and distribution along the NW axis, instead of the shape and elastic deformation of the wire.

¹⁹ Note that this approach is only correct as long as the crystal consists of complete unit cells - a reasonable approximation as long as the dimensions of the wire are much larger than the unit cell parameters.

²⁰ As the NW is much longer (several μm vs. $\approx 100 nm$), the FT of its shape is essentially 2D.

²¹ The optimization used 200 to 400 cycles, with a fixed square support more than twice the size of the NW, and was repeated 400 times to avoid stagnation.